J Electroceram (2011) 27:83–88
DOI 10.1007/s10832-009-9577-8

SPECIAL ISSUE ON ELECTROCERAM XI: THEORY AND MODELLING

Modeling of transport properties of interfacially controlled electroceramics: Application to n-conducting barium titanate

W. Preis · W. Sitte

Received: 19 September 2008 / Accepted: 28 April 2009 / Published online: 21 May 2009

Abstract Grain boundary regions in n-conducting barium titanate ($BaTiO_3$) are re-oxidized during the cooling process after sintering the ceramics in air. The kinetics of this re-oxidation process is determined by rapid transport of oxygen along the grain boundaries and slow (rate-determining) diffusion of cation vacancies from the grain boundaries into the grains until the diffusion process is frozen-in. Based on numerical calculations of frozen-in diffusion profiles of cation vacancies at grain boundary regions for various cooling rates, a modified Schottky-barrier model is introduced in order to calculate the grain boundary resistivity as a function of temperature from the Curie-point up to 900°C. A change of the activation energy at approximately 500°C is predicted owing to an enrichment of holes in the space charge layers at elevated temperatures. The modeling results are compared with experimental data for $BaTiO_3$-based positive temperature coefficient resistors (PTCRs).

Keywords Donor-doped $BaTiO_3$ · Re-oxidation kinetics · Diffusion profiles · Grain boundary resistivity · Schottky-barrier model

1 Introduction

A detailed knowledge of the electrical properties of barium titanate ceramics ($BaTiO_3$) over a wide temperature range is of considerable importance for a better understanding as well as optimization of both the processing and function of numerous electroceramic components, such as positive temperature coefficient resistors (PTCRs) or multilayer ceramic capacitors (MLCCs). Especially, donor-doped barium titanate is widely applied in PTCRs, where the resistance increases by several orders of magnitude above the ferroelectric-paraelectric phase transition temperature (Curie-point). This PTC behavior is well-known in literature and is clearly attributed to space charge effects at the grain boundaries [1–7].

The electrical properties of the grain boundaries in n-conducting $BaTiO_3$ are mainly governed by the type and concentration of interfacial point defects, e.g. segregated acceptor co-dopants or cation vacancies [8–12]. The composition of grain boundary regions depends strongly on the defect chemistry of the grain interior (bulk) as well as on preparation conditions, such as sintering temperature, dwell time, and cooling rate. The defect chemistry of donor-doped barium titanate has been treated extensively in literature [13–15]. It is generally accepted that at oxidizing conditions the donor dopants in n-type $BaTiO_3$ are compensated by acceptor co-dopants, cation vacancies, and electrons.

It is the aim of this contribution to emphasize the role played by cation vacancies formed at grain boundary regions during the re-oxidation process after sintering. The grain boundary resistivities are highly affected by these interfacial defects acting as additional acceptor states. The grain boundary resistances are calculated by application of a modified double-Schottky-barrier model and compared with experimental results for donor doped and acceptor co-doped $BaTiO_3$ ceramics of almost equal composition but different average grain sizes (microstructure). The experimental data have been obtained from impedance spectroscopy over a wide temperature range

W. Preis (✉) · W. Sitte
Chair of Physical Chemistry, University of Leoben,
Franz-Josef-Strasse 18,
A-8700 Leoben, Austria
e-mail: wolfgang.preis@mu-leoben.at

(25–900°C). The contributions of both electrons and holes to the resistivity of the grain boundary layers are taken into account.

2 Theoretical considerations

The grain boundary regions of $BaTiO_3$ based PTCR ceramics are characterized by diffusion profiles of cation vacancies which are formed due to re-oxidation during the cooling process after sintering [8]. It is still a matter of debate which type of cation vacancy ($V_{Ba}^{''}$ or $V_{Ti}^{''''}$) is predominantly created by re-oxidation [13, 14]. Since the formation of $V_{Ti}^{''''}$ seems to be more energetically favorable than the creation of $V_{Ba}^{''}$ [9], $V_{Ti}^{''''}$ will be assumed to be the predominant species in the following. According to the defect chemistry of donor-doped $BaTiO_3$ the incorporation of oxygen leads to the formation of a titania-rich phase (e.g. $Ba_6Ti_{17}O_{40}$) at the grain boundaries and cation vacancies in the bulk of barium titanate ceramics [13–15]

$$Ti_{Ti}^{\times} + O_2(g) + 4\,e' \leftrightarrow V_{Ti}^{''''} + TiO_2. \tag{1}$$

The activity of TiO_2 is fixed by the equilibrium between the titania-rich phase and barium titanate. In PTC ceramics the donor dopants, e.g. $Y_{Ba}^{\bullet}$, are partly compensated by acceptor co-dopants, e.g. $Mn_{Ti}^{'}$, $Mn_{Ti}^{''}$, and cation vacancies, e.g. $V_{Ti}^{''''}$, acting as additional (shallow) acceptor states. It should be mentioned that any valence change of cation vacancies is disregarded. The electronic charge carriers are trapped by deep acceptor states (Mn co-dopants) which are segregated at the grain boundaries [10]. Hence, the net acceptor-doped and negatively charged interfacial grain boundary core gives rise to space charge layers at adjacent net donor-doped bulk regions where the electrons are depleted. Below the ferroelectric-paraelectric transition temperature (Curie-point, T_C) the interfacial charges are almost entirely compensated by the spontaneous ferroelectric polarization, preventing the formation of distinct space charge layers and potential barriers at the grain boundaries. When the temperature is raised through the ferroelectric-paraelectric phase transition, the resistance of PTC ceramics increases rapidly by virtue of potential barriers at the grain boundaries. This double-Schottky-barrier model has been outlined in detail by numerous authors [1–5, 7]. However, the effect of diffusion profiles of cation vacancies on the grain boundary resistivity has rarely been treated in literature so far [6, 8, 16].

The re-oxidation kinetics of donor-doped barium titanate is known to be determined by extremely fast diffusion of oxygen along the grain boundaries and slow (rate-determining) bulk diffusion of cation vacancies from the grain boundaries into the grains [15, 17, 18]. As the chemical diffusion coefficient of the bulk necessary for the description of these transport processes increases strongly with increasing temperature according to an Arrhenius-law with an activation energy around 2.2–2.75 eV [17, 19], the diffusion is frozen-in below approximately 1000–1100°C [16]. Within the framework of the Schottky approximation the space charge density in the depletion zone is given by the concentrations of the immobile ionic defects (at temperatures below 900°C)

$$\begin{aligned}\rho &= e\left(\left[Y_{Ba}^{\bullet}\right] - \left[Mn_{Ti}^{'}\right] - 2\left[Mn_{Ti}^{''}\right] - 4\left[V_{Ti}^{''''}\right]\right)\\ &= en_0\mathrm{erf}(x/L_c); 0 < x < \lambda_0,\end{aligned} \tag{2}$$

with e, n_0, and λ_0 being the elementary charge, the uniform electron density of the bulk, and the depletion zone width, respectively. The diffusion profile is approximated by $\mathrm{erfc}(x/L_c) = 1 - \mathrm{erf}(x/L_c)$, where L_c is a characteristic diffusion length (penetration depth) of cation vacancies from the grain boundaries into the grains. Introducing the approximation, $\partial\phi/\partial x = 0 (x \geq \lambda_0)$, Poisson's equation

$$\frac{\partial^2\phi}{\partial x^2} = -\frac{\rho}{\varepsilon\varepsilon_0} \tag{3}$$

can be solved analytically, resulting in an expression for the space charge potential as a function of position in the depletion zone [16]

$$\begin{aligned}\phi = \phi(\lambda_0) - \frac{e\lambda_0^2 n_0}{2\varepsilon\varepsilon_0}\Bigg\{\left(1-\frac{x}{\lambda_0}\right)^2 - \frac{2L_c^2}{\lambda_0^2}\left[\mathrm{i}^2\mathrm{erfc}\left(\frac{x}{L_c}\right) - \mathrm{i}^2\mathrm{erfc}\left(\frac{\lambda_0}{L_c}\right)\right]\\ + \frac{2L_c(\lambda_0 - x)}{\lambda_0^2}\mathrm{ierfc}\left(\frac{\lambda_0}{L_c}\right)\Bigg\}.\end{aligned} \tag{4}$$

The integrated error functions are given by $\mathrm{ierfc}(x) = \exp(-x^2)/\sqrt{\pi} - x\mathrm{erfc}(x)$ and $\mathrm{i}^2\mathrm{erfc}(x) = 1/4[\mathrm{erfc}(x) - 2x\mathrm{ierfc}(x)]$, respectively, and the symbols ε_0 and $\phi(\lambda_0)$ denote the permittivity of vacuum and the space charge potential at $x=\lambda_0$. The relative permittivity obeys the Curie-Weiss law [20]

$$\varepsilon = \frac{C}{T-\theta} + \varepsilon_L \tag{5}$$

with C, ε_L, and θ being the Curie-Weiss constant, the dielectric constant extrapolated to infinite temperature, and the Curie-Weiss temperature, respectively. The potential barrier height is obtained from, $\phi_0 = |\phi(0) - \phi(\lambda_0)|$, which can be written as

$$\phi_0 = \frac{e\lambda_0^2 n_0}{2\varepsilon\varepsilon_0}\left[1 - \frac{L_c^2}{2\lambda_0^2} + \frac{2L_c^2}{\lambda_0^2}\mathrm{i}^2\mathrm{erfc}\left(\frac{\lambda_0}{L_c}\right) + \frac{2L_c}{\lambda_0}\mathrm{ierfc}\left(\frac{\lambda_0}{L_c}\right)\right]. \tag{6}$$

The density of occupied acceptor states at the grain boundary (interfacial charge density) reads [16]

$$N_s = 2n_0\left[\lambda_0 - \frac{L_c}{\sqrt{\pi}} + L_c \mathrm{ierfc}\left(\frac{\lambda_0}{L_c}\right)\right]. \tag{7}$$

The temperature dependence of the interfacial charge density is given by Fermi-Dirac statistics

$$N_s = \frac{N_{s0}}{1 + \exp\{[\varepsilon_F - e\phi(0) - \varepsilon_A]/kT\}} \tag{8}$$

where $\phi(0)$, N_{s0}, ε_F, and ε_A correspond to the space charge potential at $x=0$, the density of acceptor states at the grain boundary core (interfacial density of segregated acceptor co-dopants), the Fermi level, and the energy level of the (deep) acceptor states at the grain boundary relative to the conduction band edge, respectively. The parameters k and T have their usual meanings. The Fermi level is defined by $\varepsilon_F = kT\ln(N_c/n_0)$ and the energy level ε_A is assumed to be a linear function of temperature [7, 16]

$$\varepsilon_A = \varepsilon_A(298.15\,\mathrm{K}) + \frac{\partial\varepsilon_A}{\partial T}(T - 298.15\,\mathrm{K}). \tag{9}$$

The effective density of states of the conduction band amounts to $N_c = 1.56 \times 10^{22}\,\mathrm{cm}^{-3}$ [3, 5]. It is worthwhile mentioning that trapping of electrons by acceptor states in the boundary layer is accompanied by a valence change between Mn^{4+} and Mn^{3+}, such that the energy level of the acceptor states is related to their standard chemical potentials [21], i.e. $\varepsilon_A = \mu^\circ(Mn^{4+}) - \mu^\circ(Mn^{3+})$. At temperatures below approximately 200°C Mn^{2+} states may likewise become important in the core regions. In the bulk the Mn co-dopants are almost entirely in the valence state Mn^{2+} even at high temperatures owing to the fairly high bulk electron concentration [19], such that the effective donor concentration is given by $[D^\bullet]_{eff} = [Y^\bullet_{Ba}] - 2[Mn''_{Ti}]$.

The spatial dependence of the charge carrier densities of electrons, $n(x)$, and holes, $p(x)$, in the space charge layer is given by

$$n(x) = n(\lambda_0)\exp\{e[\phi - \phi(\lambda_0)]/kT\} \tag{10a}$$

and

$$p(x) = \frac{N_c N_v}{n(\lambda_0)}\exp(-\varepsilon_g/kT) \times \exp\{-e[\phi - \phi(\lambda_0)]/kT\}, \tag{10b}$$

where ε_g, N_c, and N_v are the band gap energy and the effective densities of states in the conduction and valence band, respectively. The electron density at $x=\lambda_0$ can be expressed as $n(\lambda_0) = n_0\mathrm{erf}(\lambda_0/L_c)$ by virtue of Eq. (2). Whereas the electrons are depleted in the space charge layers, the holes are enriched in accordance with Eq. (10) [22]. The grain boundary resistance is then obtained from

$$R_{gb} = \frac{2l}{Ad_g}\int_0^{\lambda_0}\frac{\mathrm{d}x}{eb_e n(x) + eb_h p(x)} \tag{11}$$

by taking into account the contributions of both depleted electrons and enriched holes. The quantities A, l, d_g, b_e, and b_h denote the area of the cross section and thickness of the ceramic sample, the average grain size, and the spatially invariant mobilities of electrons and holes, respectively. The linearly approximated space charge potential can be written as

$$\phi = \phi(\lambda_0) - \phi_0 + \frac{eN_s}{2\varepsilon\varepsilon_0}x \tag{12}$$

by combining Eqs. (4), (6), and (7). Inserting Eqs. (10a), (10b), and (12) into Eq. (11) and evaluating the integral one finally arrives at

$$R_{gb} = \frac{l}{d_g A}\left(\frac{4\varepsilon\varepsilon_0 kT}{e^2 N_s}\right)\frac{\exp\left[\varepsilon_g/(2kT)\right]}{e\sqrt{N_c N_v b_e b_h}} \times \\ \times\left\{\arctan\left[\frac{n(\lambda_0)}{\sqrt{N_c N_v}}\sqrt{\frac{b_e}{b_h}}\exp\left(\frac{\varepsilon_g/2 - e\phi_0}{kT}\right) \times \exp\left(\frac{e^2 N_s\lambda_0}{2\varepsilon\varepsilon_0 kT}\right)\right] - \right. \\ \left. - \arctan\left[\frac{n(\lambda_0)}{N_c N_v}\sqrt{\frac{b_e}{b_h}}\exp\left(\frac{\varepsilon_g/2 - e\phi_0}{kT}\right)\right]\right\}. \tag{13}$$

It should be noted that Eq. (13) is valid as long as the space charge density [Eq. (2)] is not remarkably affected by the enriched holes in the space charge layer. Furthermore, any contributions of the core region, containing the segregated negatively charged interfacial acceptor states, to the grain boundary resistance have likewise been neglected.

3 Results and discussion

The electrical properties of two PTC resistors (samples have been provided by EPCOS) of almost equal dimensions and composition but different microstructure (average grain size: 2.8 and 6.6 µm, respectively) were investigated by impedance spectroscopy between room temperature and 900°C [23]. The bulk and grain boundary resistances are plotted as a function of temperature in Fig. 1. The PTC effect (rapid increase of the grain boundary resistance by several orders of magnitude) can be observed between 90 and 200°C which is caused by the formation of Schottky-barriers at the grain boundaries above the Curie point ($T_C \approx$ 90°C) [7]. The Curie-point is somewhat diminished compared to pure $BaTiO_3$ owing to A-site doping with

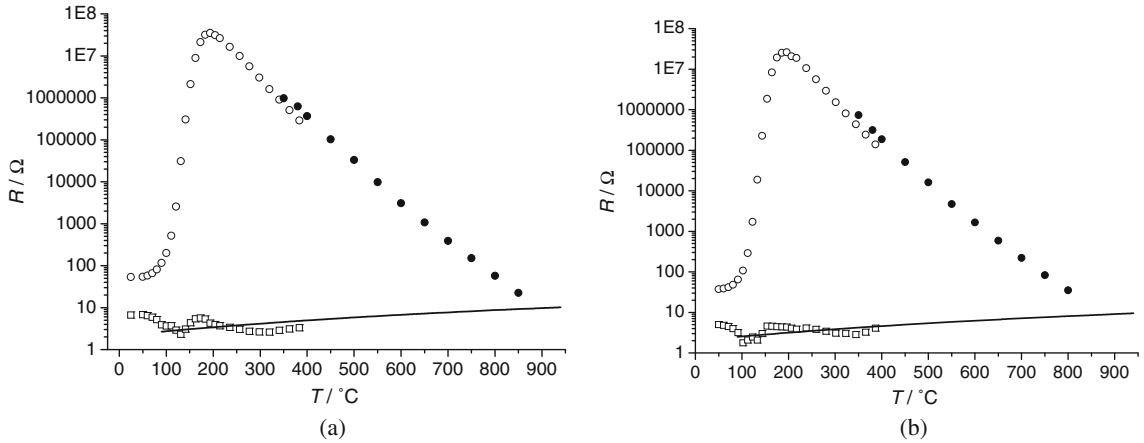

Fig. 1 Bulk and grain boundary resistances as a function of temperature. (□) Bulk and (○) grain boundary resistances obtained by application of NiCr/Ag–electrodes [7]. (●) Grain boundary resistances obtained by application of Pt–electrodes [23]. Solid line: calculated bulk resistances for the paraelectric phase with n_0=2.0×10^{18} cm^{-3} and the temperature dependent mobility of electrons taken from Ref. [24]. (**a**) Sample 1 with average grain size: 2.8 µm; diameter: 8.03 mm; thickness: 2.06 mm. (**b**) Sample 2 with average grain size: 6.6 µm; diameter: 7.92 mm; thickness: 2.29 mm

Table 1 Optimized parameters of the modified Schottky-barrier model for L_c=0.20 µm in accordance with Ref. [16].

Sample (x_{Sr}/x_{Pb}≈1.6)	d_g (µm)	N_{s0} (cm^{-2})	ε_A(298.15K) (eV)	$(\partial\varepsilon_A/\partial T)$ (eVK^{-1})	θ (K)	ε_A(573.15K) (eV)
1	2.8	7.44×10^{13}	1.20	6.99×10^{-4}	345.5	1.39
2	6.6	7.77×10^{13}	1.23	6.00×10^{-4}	349.9	1.39

Table 2 Additional parameters of the modified Schottky-barrier model.

	ε_g (eV)	N_c (cm^{-3})	N_v (cm^{-3})	b_h ($cm^2V^{-1}s^{-1}$)	n_0 (cm^{-3})
Parameter	3.15	1.56×10^{22}	6.80×10^{22}	0.08	2.0×10^{18}
Reference	[26]	[3, 5]	[26]	[26]	[16]

b_e / cm^2 $V^{-1}s^{-1}$ =7356 $(T/K)^{-3/2}$ ×exp(−0.063 eV / 3 kT) in accordance with Ref. [24]

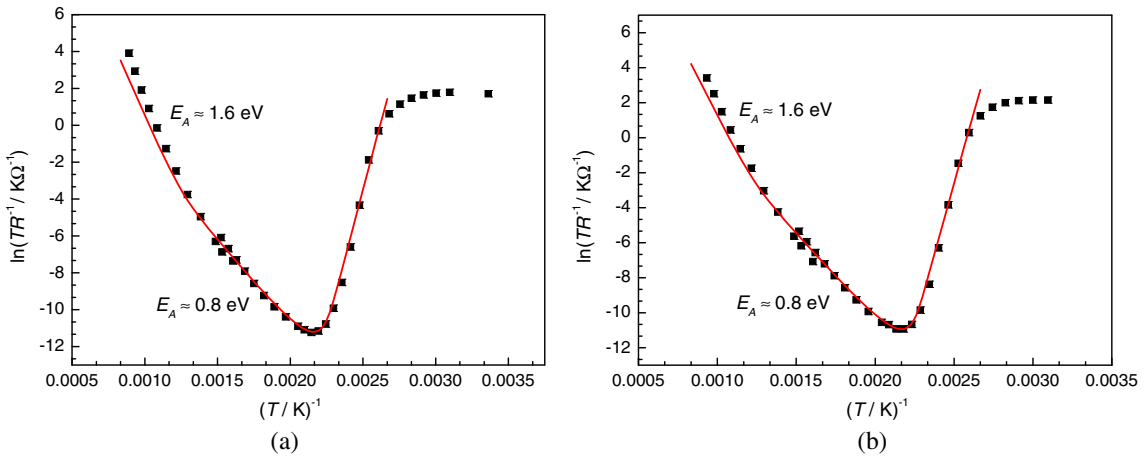

Fig. 2 Arrhenius plots of the grain boundary resistances. (■) experimental data obtained from impedance spectroscopy [7, 23]. Solid lines have been calculated by application of the modified Schottky-barrier model [Eq. (13)], parameter values are listed in Tables 1 and 2. (**a**) Sample 1 with average grain size: 2.8 µm; diameter: 8.03 mm; thickness: 2.06 mm. (**b**) Sample 2 with average grain size: 6.6 µm; diameter: 7.92 mm; thickness: 2.29 mm

strontium and lead ($x_{Sr}/x_{Pb}\approx1.6$). The bulk resistivity shows a weak temperature dependence with typical values around 10Ω cm. Taking the temperature dependent electron mobility from Ref. [24] the electron density of the bulk is estimated to be $n_0=2.0\times10^{18}\,cm^{-3}$. Above 200°C the grain boundary resistances decrease considerably with increasing temperature (NTC regime). It should be mentioned that the defect chemistry of n-conducting $BaTiO_3$ is frozen-in below 1000°C [16], such that all measurements (25–900°C) do not refer to samples equilibrated with the surrounding gas phase (air).

A comprehensive model for the temperature dependence of the grain boundary resistivity in the temperature regime between the Curie-point and approximately 400°C has been proposed, recently [16]. The diffusion profiles of cation vacancies acting as additional (shallow) acceptor states in the space charge layer are properly taken into account. A parameter set for N_{s0}, ε_A(298.15 K), $\partial\varepsilon_A/\partial T$, and θ has been obtained by application of a least squares fitting procedure to the experimental data from 90 to 400°C, adopting $L_c=0.20\,\mu m$ for the characteristic diffusion length (penetration depth) of the cation vacancies, see Table 1. The parameters C and ε_L have been taken from Refs. [25] and [20]; $C=1.5\times10^5$ K and $\varepsilon_L=44$. At temperatures fairly close to the phase transition temperature (Curie-point) ε_L can usually be omitted. Using these quantities and appropriate literature data for ε_g, N_c, N_v, b_e, and b_h (see Table 2), Eq. (13) can be employed for the prediction of the temperature dependence of the grain boundary resistance over a wide temperature range (up to 900°C), taking account of a significant enrichment of holes in the space charge layer at elevated temperatures. Figure 2 shows a comparison of the experimental data with the present space charge model. It is worth mentioning that the experimental values are remarkably well predicted by the present model [Eq. (13)]. The PTC effect can be interpreted in terms of a tremendous increase of the potential barrier height with increasing temperature. At temperatures above 200°C the potential barrier height is almost constant due to the interplay between the decreasing dielectric constant [Eq. (5)] and the decreasing density of occupied acceptor states in the grain boundary core region [Eq. (8)], see Refs. [7] and [16] for more details. The almost constant barrier height gives rise to the NTC behavior above 200°C, where the activation energy is given by $E_A\approx e\phi_0\approx0.8$ eV. However, the Arrhenius-plots in Fig. 2 reveal that at approximately 500°C the activation energy increases from 0.8 eV to 1.6 eV$\approx\varepsilon_g/2$. The increase of the activation energy from $e\phi_0$ to $\varepsilon_g/2$ can clearly be attributed to the enrichment of holes in the space charge layer [22].

Figure 3 shows concentration profiles of point defects in the space charge layers at the grain boundaries. The strong depletion of electrons leads to the formation of a potential

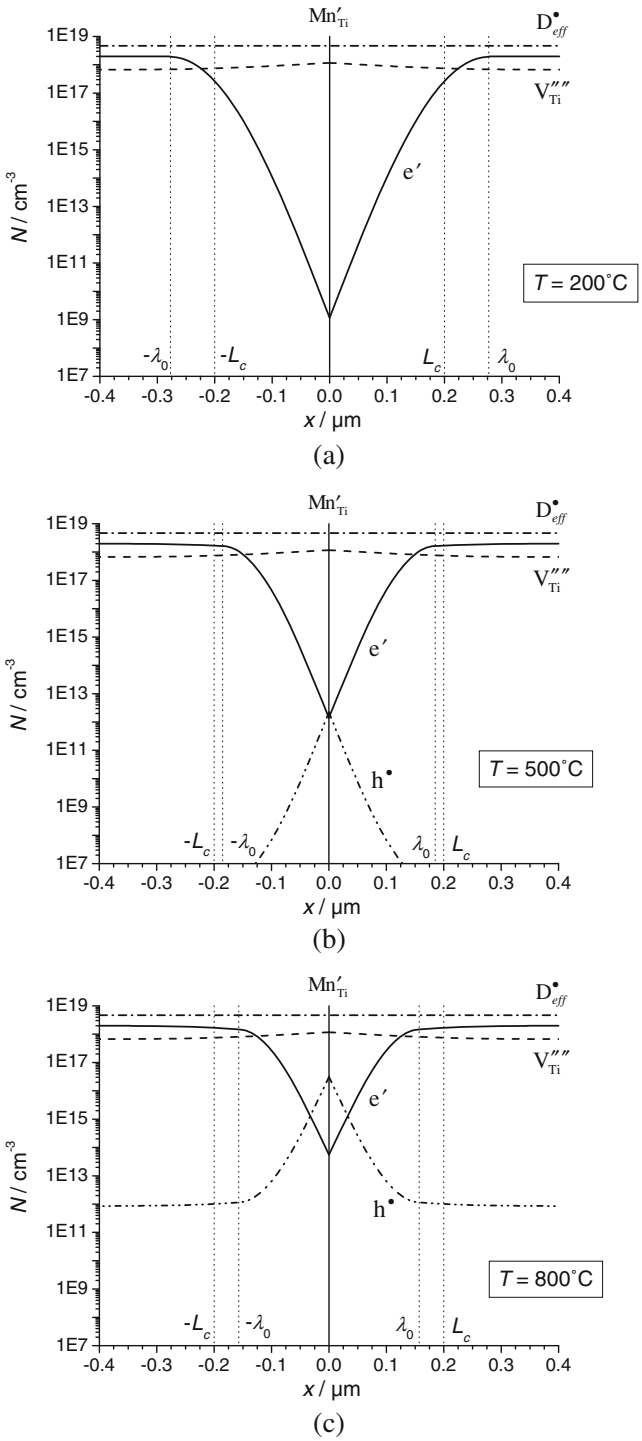

Fig. 3 Concentration profiles of point defects at the grain boundaries in accordance with the present Schottky-barrier model. The acceptor co-dopants are segregated at the core region, the diffusion profiles of the Ti-vacancies are frozen-in, the electrons are depleted while the holes are enriched in the space charge layers. (**a**) T=200°C. (**b**) T=500°C. (**c**) T=800°C

barrier at the grain boundaries of n-conducting $BaTiO_3$. The enrichment of holes can be disregarded between the Curie-point and temperatures up to 400–500°C owing to the high band gap energy of 3.15 eV. On the contrary, at temperatures above 500°C the enrichment of holes in the space charge layer significantly affects the NTC regime, resulting in an increase of the activation energy. Moreover, it should be mentioned that the space charge density is not spatially uniform, which is in accordance with the present modified Schottky-barrier model where diffusion profiles of cation vacancies are taken into account.

4 Summary

Both the PTC effect and the temperature dependence of the grain boundary resistances in the NTC regime up to 900°C are satisfactorily described for PTC resistors of equal dimensions and composition but different microstructure by application of a modified double-Schottky-barrier model. Apart from deep acceptor states corresponding to segregated acceptor co-dopants in the core regions of the grain boundaries, diffusion profiles of cation vacancies acting as additional (shallow) acceptor states at grain boundary regions are taken into account. These diffusion profiles are formed during the cooling process after sintering the PTC ceramics. At fairly high temperatures (above 500°C) the grain boundary resistivity of n-type $BaTiO_3$ is strongly affected by enriched holes in the space charge layers which give rise to a change of the activation energy from 0.8 eV to 1.6 eV.

Acknowledgements The authors wish to thank A. Bürgermeister for performing the impedance measurements. Financial support by the Austrian Federal Government and the Styrian Provincial Government, represented by Österreichische Forschungsförderungsgesellschaft mbH and Steirische Wirtschaftsförderungsgesellschaft mbH, within the research activities of the K2 Competence Centre on "Integrated Research in Materials, Processing and Product Engineering", operated by the Materials Center Leoben Forschung GmbH under the frame of the Austrian COMET Competence Centre Programme, is gratefully acknowledged.

References

1. W. Heywang, J. Am. Ceram. Soc. **47**, 484 (1964). doi:10.1111/j.1151-2916.1964.tb13795.x
2. W. Heywang, J. Mater. Sci. **6**, 1214 (1971). doi:10.1007/BF00550094
3. G.H. Jonker, Solid-State Electron. **7**, 895 (1964). doi:10.1016/0038-1101(64)90068-1
4. B.M. Kulwicki, A.J. Purdes, Ferroelectrics **1**, 253 (1970)
5. H. Ihrig, W. Puschert, J. Appl. Phys. **48**, 3081 (1977). doi:10.1063/1.324078
6. K. Hayashi, T. Yamamoto, Y. Ikuhara, T. Sakuma, J. Appl. Phys. **86**, 2909 (1999). doi:10.1063/1.371140
7. W. Preis, A. Bürgermeister, W. Sitte, P. Supancic, Solid State Ion. **173**, 69 (2004). doi:10.1016/j.ssi.2004.07.054
8. J. Daniels, R. Wernicke, Philips Res. Repts. **31**, 544 (1976)
9. G.V. Lewis, C.R.A. Catlow, R.E.W. Casselton, J. Am. Ceram. Soc. **68**, 555 (1985). doi:10.1111/j.1151-2916.1985.tb11523.x
10. Y.-M. Chiang, T. Takagi, J. Am. Ceram. Soc. **73**, 3286 (1990). doi:10.1111/j.1151-2916.1990.tb06451.x
11. A.B. Alles, V.L. Burdick, J. Am. Ceram. Soc. **76**, 401 (1993). doi:10.1111/j.1151-2916.1993.tb03798.x
12. M.M. Gallego, A.R. West, J. Appl. Phys. **90**, 394 (2001). doi:10.1063/1.1374476
13. J. Daniels, K.H. Härdtl, Philips Res. Repts. **31**, 489 (1976)
14. D.M. Smyth, J. Electroceramics **9**, 179 (2002)
15. H.-I. Yoo, C.-E. Lee, J. Am. Ceram. Soc. **88**, 617 (2005). doi:10.1111/j.1551-2916.2005.00123.x
16. W. Preis, W. Sitte, Solid State Ion. **177**, 2549 (2006). doi:10.1016/j.ssi.2006.06.003
17. R. Wernicke, Philips Res. Repts. **31**, 526 (1976)
18. W. Preis, W. Sitte, J. Phys. Chem. Solids **66**, 1820 (2005). doi:10.1016/j.jpcs.2005.09.047
19. W. Preis, W. Sitte, Solid State Ion. **177**, 3093 (2006). doi:10.1016/j.ssi.2006.07.053
20. G. Rupprecht, R.O. Bell, Phys. Rev. **135**, A748 (1964). doi:10.1103/PhysRev.135.A748
21. J. Maier, Z. Phys. Chem. **219**, 35 (2005). doi:10.1524/zpch.219.1.35.55018
22. R. Waser, R. Hagenbeck, Acta Mater. **48**, 797 (2000). doi:10.1016/S1359-6454(99)00367-5
23. A. Bürgermeister, *Bulk and Grain Boundary Transport in Perovskite Oxides*, PhD thesis (University of Leoben, Austria, 2005)
24. H. Ihrig, J. Phys, C. Solid State Phys. **9**, 3469 (1975). doi:10.1088/0022-3719/9/18/013
25. C.J. Johnson, Appl. Phys. Lett. **7**, 221 (1965). doi:10.1063/1.1754387
26. H.-I. Yoo, C.-R. Song, D.-K. Lee, J. Electroceramics **8**, 5 (2002)